

# CVD-Diamond Detectors for Spectroscopy and Timing

E. Berdermann<sup>1</sup>, A. Caragheorgheopol<sup>2</sup>, M. Ciobanu<sup>1</sup>,  
B. E. Fischer<sup>1</sup>, W. Hartmann<sup>1</sup>, A. Martemiyarov<sup>1</sup>, P. Moritz<sup>1</sup>,  
J. Morse<sup>3</sup>, M. Pomorski<sup>1</sup>, M. Salomé<sup>3</sup>  
*for the NoRHDia Collaboration\**

<sup>1</sup>GSI Darmstadt, <sup>2</sup>IFIN-HH Bucharest, <sup>3</sup>ESRF Grenoble,  
INFN University of Milan, Limburgs Universitaer Centrum,  
CEA LIST Saclay, DESY Zeuthen, Technical University of Munich,  
CERN Geneva, University of Karlsruhe, IJS Ljubljana,  
VERA Laboratory Vienna, Wits University of Johannesburg

## Abstract

The suitability of single-crystal diamond made by chemical vapour deposition for particle identification in heavy-ion experiments and for precise timing of relativistic ions and minimum-ionizing protons is investigated. Characterisation data of various samples and their influence to the detector performance are discussed. The lifetime of the charge carriers is found to be much longer than the transition time of the particle-generated charge through the detector, confirming the complete charge collection measured with both, traversing high-energetic electrons from <sup>90</sup>Sr sources and stopped alpha particles from mixed-nuclide sources. For such  $\alpha$ -particles of a mean energy around 5.5 MeV, an energy resolution  $\Delta E = 17$  keV (FWHM) is measured. The flat-top timing signals show commonly uniform rise times  $< 200$  ps limited only by the electronics bandwidth. The drift velocity of electrons at operation bias is  $v_{dr}^e \sim 80$   $\mu\text{m}/\text{ns}$ , whereas holes drift with  $v_{dr}^h = 100$   $\mu\text{m}/\text{ns}$ . Thus, the expected count-rate capability of a detector with a thickness in the order of 300  $\mu\text{m}$  amounts to  $10^8$  particles /s.

---

\* Supported by EC, Project RII3-CT-2004-506078

## 1 Introduction

The polycrystalline texture of CVD-diamond sensors available so far [1][2][3] leads to a position-dependent and incomplete charge collection preventing their use for particle identification via energy- or energy-loss measurements, time-of-flight measurements of Minimum-Ionizing Particles (MIPs), as well as for any application performed with highly focussed beams. However, a variety of current and future experiments projected e.g. for SIS and FAIR in Darmstadt, TESLA at DESY, SLHC at CERN or ESRF in Grenoble, require radiation-hard detector devices of such properties. In addition, stimulated by Heavy-Ion (HI) timing results published for Poly Crystalline CVD-Diamond Detectors (PC-DD) [3], an increasing interest from the low-energy nuclear-physics domain is noticed.

Recently, the quality of CVD diamond has been tremendously improved. Growth processes where the previous used silicon {1 0 0} wafers are replaced by high-pressure high-temperature single-crystal diamond substrates provide a monocrystalline material almost free of structural defects and chemical impurities. In section 3, common features of early Single-Crystal CVD-Diamond Detectors (SC-DD) are reported and compared to those of competitive devices, which are silicon detectors if energy resolution is concerned and, PC-DD whenever high-rate counting and precise timing is considered. Particular care is taken over the cleaning of the diamond and its metallization, both of which influence the detector behaviour (section 2). The systematic characterisation of a detector as large as  $3.5 \times 3.5 \times 0.393 \text{ mm}^3$  is reported in section 4. A summary of the R&D status is given in section 5, including remarks for the implementation of CVD-diamond detectors in hadron physics experiments.

## 2 Diamond Sample Preparation

The treatment of samples before, during, and after evaporation or sputtering of the multilayer electrodes appears to be the most crucial issue in the SC-DD manufacture. The choice of metals is decisive for the formation of either a Schottky barrier - if for instance Cr/Au or pure aluminium metallization is chosen - or of a contact of ohmic behaviour if carbide-forming Titanium followed by Pt/Au layers is applied [4]. Effects arising from space charges that are present in the interface to the diamond depend on the type of residual conductivity of surface- and bulk material, both initially unknown. A Schottky junction in an n-type semiconductor gives rise to an electron depletion layer and in a p-type semiconductor to a hole depletion layer, respectively. PC-CVDD has been characterized as n-type material [4].

The samples are boiled in Aqua Regia and Sulfo-Chromic acid ( $\text{CrO}_3 + \text{H}_2\text{SO}_4$ ) to obtain diamond surfaces free of impurities and graphite, the last being highly p-conductive. The resultant resistivity of the films should increase by several orders of magnitude [4]. We are testing consecutively the detector behaviour with

different contacts, including combinations of one Schottky- and one Ohmic electrode. Probably due to the lower quality or a different surface reconstruction, no influence to the PC-DD performance has been observed in the past applying various types of electrodes described above.

### 3 Features of Early Single-Crystal CVD-Diamond Detectors

In this section test data of various SC-DDs are presented - all of them provided courtesy of Reference[5]. They are identified as D1, D2, D3, and D4 of dimensions  $v_1=3.5 \times 4.3 \times 0.440 \text{ mm}^3$ ,  $v_2=3 \times 3 \times 0.295 \text{ mm}^3$ ,  $v_3=3 \times 3 \times 0.345 \text{ mm}^3$  and  $v_4=3.5 \times 3.5 \times 0.393 \text{ mm}^3$ , respectively. The nominally intrinsic diamond material is metallized in all cases with simple sandwich-dot electrodes consisting of 500 Å chromium- and 1000 Å gold layers, forming the active detector areas  $a_1 = a_4 = 4.9 \text{ mm}^2$  respective  $a_2 = a_3 = 3.14 \text{ mm}^2$ .

#### 3.1 Dark-Current Characteristics

Precise three pole electrometer measurements are performed in darkness under nitrogen flow. The set up consists of a Teflon barrel mounted inside an aluminium housing at ground potential. Parasitic currents caused by humidity or air ionization are minimized and distortion of the measurement by pick-up is thus eliminated.

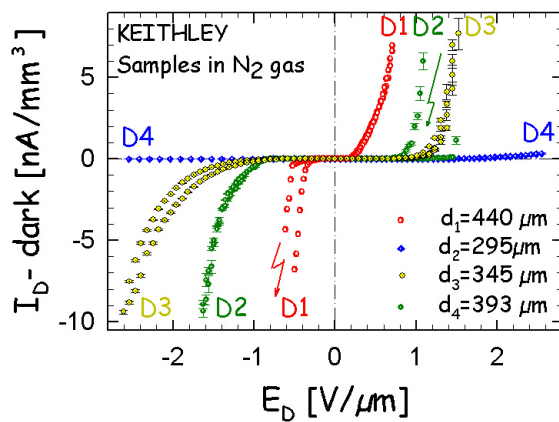


**Figure 1:**

Dark-current characteristics of samples D1-D4. Only D4 shows the expected behaviour of negligible current well below  $1 \text{ nA/mm}^3$  over a range of  $E_D = \pm 2 \text{ V/}\mu\text{m}$ . In the case of D1-D3, surface conductivity or effects from the contact interface to the detectors are indicated.

Figure 1 shows the electric field dependence of dark currents  $I_{D1-D4}$  normalized to the active detector volume. The expected desirable characteristics are found only for sample D4. Lowest currents of absolute values well below  $1 \text{ nA/mm}^3$  are measured over a wide field range  $> \pm 2 \text{ V/}\mu\text{m}$ . Samples D1-D3 on the other hand, show increasing current at lower bias than good 'As Grown' (AG) electronic grade PC-DDs[3]. Moreover, real break down occurs occasionally (D1-D3 "lightning bolts") and persistent hysteretic behaviour is observed afterwards. These data, obtained from such high-resistivity ( $>10^{14} \text{ }\Omega\text{cm}$ ) material, are not understood yet. Surface conductivity or contact effects (section 2) are indicated, which require detailed investigation. The present layout of simple dot electrodes

will be replaced by metallization with guard ring structures, allowing in the future diagnosis of surface contributions to the bulk leakage current.

## 3.2 Homogeneity of the Detector Response

### 3.2.1 Mapping with 5 keV X-Ray beams

Detector D2 has been irradiated at ID21/ESRF Grenoble with a focussed ( $0.4 \times 0.9 \mu\text{m}^2$ ) 5 keV X-ray beam of an intensity of  $\sim 10^8$  photons/s. The beam was scanned parallel to the  $\{100\}$  direction of the diamond lattice in a  $20 \mu\text{m}$  pitch raster, 0.1 s/point. Figure 2 shows the Charge-Collection Efficiency (CCE) map obtained. The circular bright-yellow area indicates the detector response from the active area of 2 mm in diameter. Besides on scratch marks of the metallization and some regions of lower response at bottom right, which disappear at higher bias, the detector is fairly homogeneous. In any case, the superior quality of SC-D2 is demonstrated convincingly by comparing the map of a PC-DD (black and white onset, bottom left) in same spatial scale. The granular growth of this type of diamond, consisting of SC-like, high-efficiency grains (bright grey) separated by regions of very-low response (grain boundaries, black and dark grey)[6] is the reason for the poor energy resolution and the significantly reduced CCE reported for PC-DDs [1][2][3].

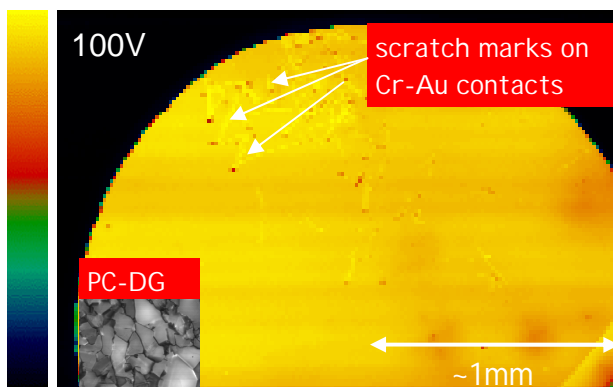


**Figure 2:** CCE maps measured with highly focussed 5 keV X-ray beams,  $\sim 10^8$  X/sec. The circular bright area of 2 mm in diameter indicates even response for the active volume of D2, whereas the black and white map (onset bottom left) reveals the granular growth of a PC-DG sample, being the reason for the significantly reduced CCE of PC-DDs. Both maps are shown at same spatial scale.

### 3.2.2 Mapping with $^{12}\text{C}$ ions

In a recent experiment at GSI's micro-beam facility, stopped  $^{12}\text{C}$  ions of two different kinetic energies were used in order to investigate distinct regions at corresponding Bragg maxima within the bulk material of detector D3. Carbon ions of 3.6 MeV/amu and 9.515 MeV/amu were chosen, leading to ion ranges of  $27 \mu\text{m}$  and  $126 \mu\text{m}$  respectively. The beam was scanned in a  $1 \mu\text{m}$  raster, applying approximately 10 ions /hit/scan. The irradiated area was  $140 \mu\text{m} \times 93 \mu\text{m}$  in the case of 3.6 A MeV beam energy and  $90 \mu\text{m} \times 60 \mu\text{m}$  in the case of 9.515 A MeV ions. Figure 3 shows the collected-charge maps obtained integrating 10 scans at each energy. The uniformly distributed micro-pattern is unavoidable binning

artefact. Thus, good homogeneity of the bulk material within the investigated ion range is demonstrated for this sample too (compare sect. 3.2.1).

An additional parameter sensitive to high CCE and homogeneity of the detectors is the energy resolution measured with such mono-energetic charged particles. Charge losses, if existing, are randomly distributed and would broaden the lines, as is found for PC-DDs[3]. The Z-data of both plots in Fig. 3 have been calibrated in MeV and plotted in Fig. 4 versus the beam energy.

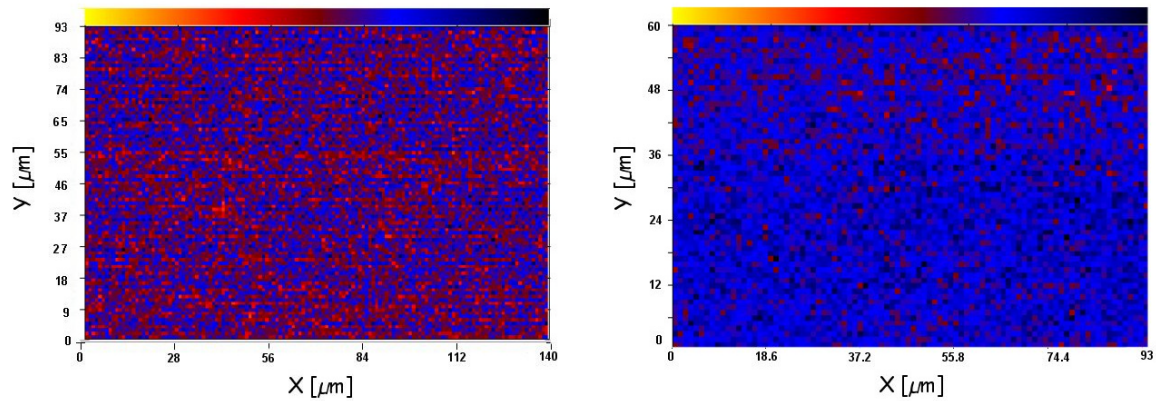


**Figure 3:** Collected charge maps of sample D3 at 1.2 V/μm, obtained from layers at 27 μm depth (left plot) and 126 μm depth (right plot). The uniformly distributed micro-pattern is unavoidable binning artefact. Dominant colours indicate the most probable charge collected, corresponding to a total energy deposit of 43.2 MeV (left plot, red) and 114.2 MeV (right plot, blue).

The FWHM of both spectral lines in Fig. 4 corresponding to relative resolutions  $\Delta E/E = 0.01$  for the energy deposit of 43.2 MeV (left peak) and  $\Delta E/E = 0.007$  for 114.2 MeV (right peak), confirm convincingly the conclusion of bulk homogeneity of detector D3.

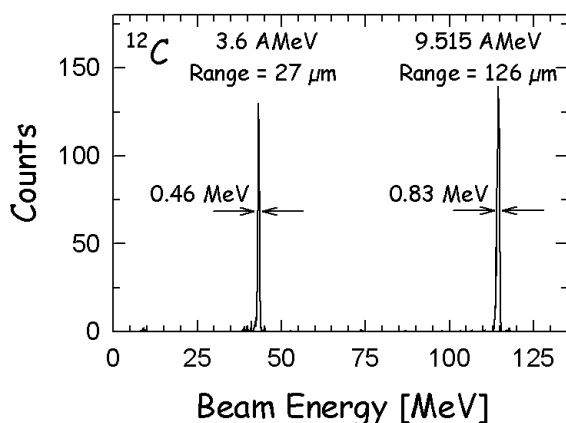


**Figure 4:** Energy spectra obtained from stopped  $^{12}\text{C}$  ions probing different layers inside D3: in  $27 \pm 5 \mu\text{m}$  depth (left line) and  $126 \pm 10 \mu\text{m}$  (right line), respectively. The homogeneity of the sample is mirrored in the resolution of  $\Delta E/E = 0.01$  for  $E = 43.2 \text{ MeV}$ , respective  $\Delta E/E = 0.007$  for  $E = 114.2 \text{ MeV}$ .

### 3.2.3 The Original CVD-Diamond Response

The original ultra-fast diamond response to an impinging charged particle is

studied using a broadband measurement system transmitting both, the high- and low-frequency components of the electrical signals almost without attenuation. The system consists of a DBA [7] amplifier operating linearly between 1 MHz and 2.3 GHz, and a Digital Sampling Oscilloscope (DSO) of 3 GHz bandwidth and sampling rate of 20 GS/s.

Short-range  $^{241}\text{Am}$  alphas provide a means of investigating separately both, electron- and hole signals. Positive bias on the  $\alpha$ -penetrated and collecting electrode (amplifier side) enables measurement of hole drift, whereas negative bias measures the signal from electron drift only. Figure 5 shows  $\alpha$ -induced signals in D2 (solid lines, 295  $\mu\text{m}$ ) and in a polished Detector Grade (DG) PC-DD (dashed lines, 500  $\mu\text{m}$ ) at same external field  $E_D = -1 \text{ V}/\mu\text{m}$ . The corresponding average pulses are overlaid in bold solid lines.

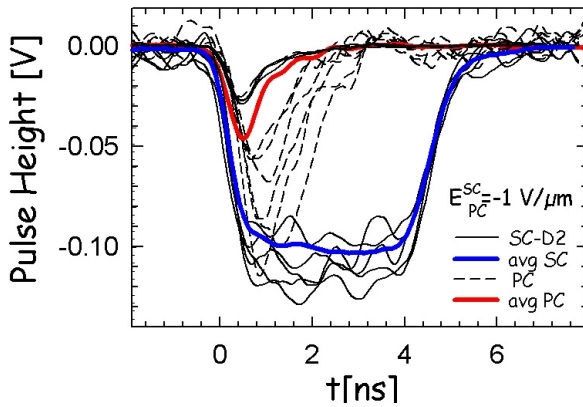


**Figure 5:** Electron drift signals in D2 (solid lines, 295  $\mu\text{m}$ ) and in a PC-DG-DD (dashed lines, 500  $\mu\text{m}$ ), respectively. The trapezoidal shape of the SC pulses show obviously constant charge drift to the opposite electrode, whereas the triangular shaped PC signals indicate severe charge trapping within the diamond bulk.

The triangular shaped PC signals of different amplitudes ( $A_{\text{avg}} \sim 0.3 \times A_{\text{max}}$ ) mirror the short drift of generated electrons in a non-homogeneous electric field before they become trapped in defects of the bulk material. Looking at its signal time response, the superior quality of SC diamond is obvious. The trapezoidal shaped pulses of similar amplitude demonstrate full charge drift to the opposite electrode within a homogeneous electric field. The pulses of both detector types show short rise time = 200 ps, but D2 collects all generated charge, which is given by the area integrated under the signal pulse. This picture reveals the common features of SC-CVD-DDs: good timing- and spectroscopic properties.

## 4 Systematic Characterisation of Detector D4

### 4.1 Pulse-Shape Parameters

The development of electron- and hole drift signals in D4 (393  $\mu\text{m}$ ) with increasing electric field is shown in Figure 6. For hole drift, the detector achieves its best performance at lower bias than is the case of electron drift. The pulse-shape parameters plotted for both cases in Fig. 7a confirm a slightly improved behaviour when operating in the hole-drift mode. However, this figure

demonstrates the speed of the detector for both polarities of the applied electric field, revealing the limits of the available electronics used. The ultra-fast rise and decay of the signals at high fields is limited by the measurement system, contributing 197 ps to the shape parameters. The same conclusion has been made for PC-DDs[3].

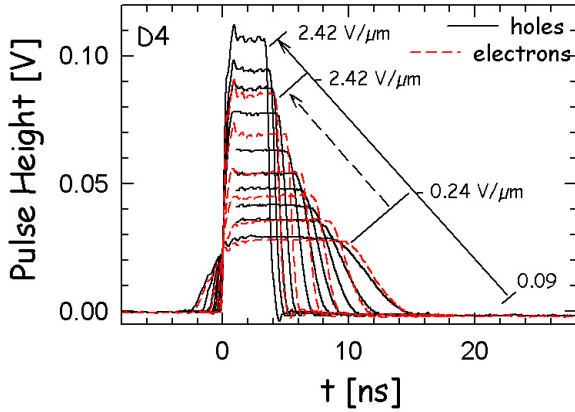


**Figure 6:** The development of  $\alpha$ -induced electron- (dashed lines) and hole (solid lines) drift signals in D4 (393  $\mu\text{m}$ ), showing the influence of increasing the external electric field  $E_D$  (given as plot parameter). Each signal is averaged over 500 single shots.

In Figure 7b the calculated rate capability of D4 is plotted over the electric field. The conclusion is that using a SC-DD of a thickness around 300 – 400  $\mu\text{m}$  at best performance, one can measure rates as high as  $3 \times 10^8$  particles/s. A PC-AG-DD used with heavy ions however, achieves  $10^9$  particles/s[3].

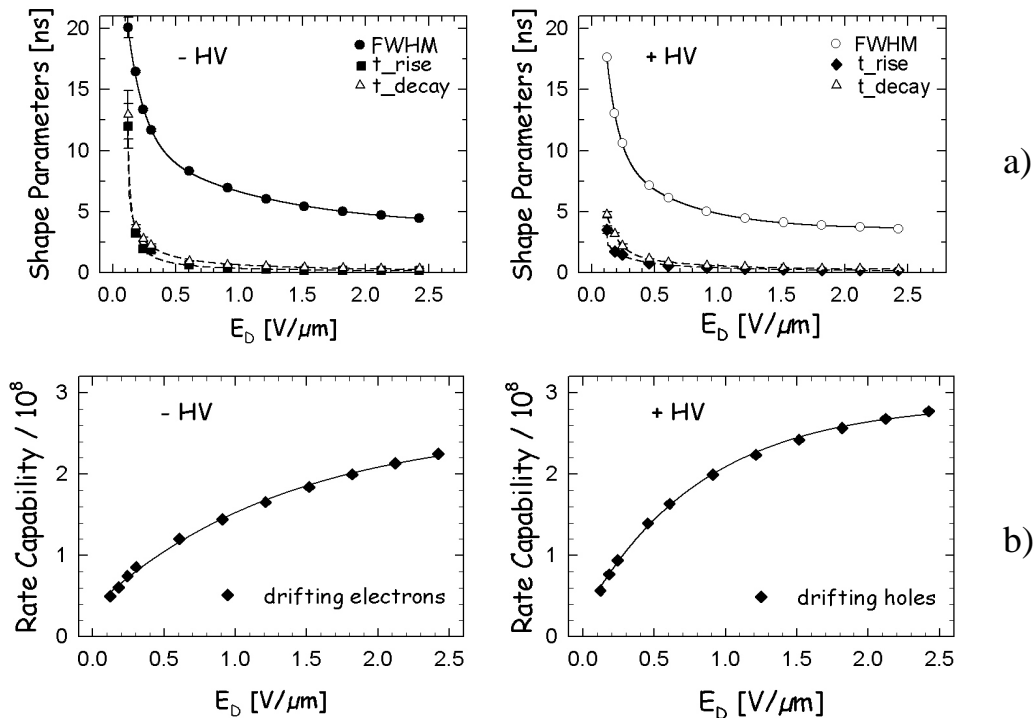


**Figure 7:** a) The dependence of the pulse shape parameters for electron- (top left) and hole-drift (top right) on the external electric field  $E_D$ . Fits and lines should guide the eyes. Values at higher fields are affected by the limiting bandwidth of electronics. b) The expected rate capability of D4 at best condition amounts to almost  $3 \times 10^8$  particles /s.

## 4.2 Drift velocity

Assuming the FWHM of the average signals presented in Fig. 6 as the transit time  $t_{TR}$  of the charge-cloud centre to the opposite electrode, the average carrier drift velocity  $v(E_D) = d_D/t_{TR}(E_D)$  has been calculated and the results are plotted in Figure 8 versus the electric field. It is remarkable that holes are drifting faster than electrons. A similar trend is observed in all SC samples tested so far. We suggest that there is either weak electron trapping in the bulk, or an effect belonging to contact problems.

The drift velocity increases proportionally to the electric field at low field strength and saturates at higher fields. The saturation velocity is not reached in this sample, neither for electrons nor for holes. Velocity data are well described [8][9][10][11] by equation (1) as proposed in [8]

$$v_{dr}(E_D) = \frac{\mu_0 E_D}{1 + \frac{\mu_0 E_D}{v_{sat}}} \quad (1)$$

with  $\mu_0$  = low-field mobility,  $v_{sat}$  = saturation velocity and  $E_D$  = electric field.

The fit provides an easy way to extract  $\mu_0$  and  $v_{sat}$ , which are parameters difficult to determine experimentally. For sample D4 we obtained:  $\mu_0^h = 2407$  [cm<sup>2</sup>/Vs],  $\mu_0^e = 1716$  [cm<sup>2</sup>/Vs] and the saturation velocities  $v_{sat}^h = 1.4 \cdot 10^7$  [cm/s],  $v_{sat}^e = 1.1 \cdot 10^7$  [cm/s]. The data are in excellent agreement with Reference[9]. However, these parameters are controversial, as discussed in the literature[12].

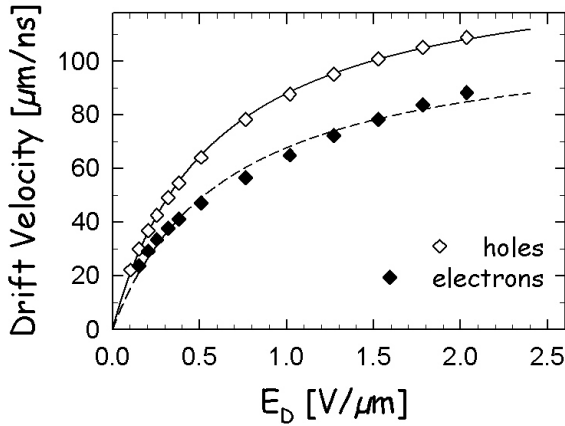


**Figure 8:** Electric field dependence of the drift velocity of the charge carriers. Both types of carriers do not achieve saturation velocity.

## 4.3 Energy Resolution and Conversion Factor e<sup>D4</sup>

<sup>12</sup>C micro-beam data as presented in section 3 is convincing evidence of the spectroscopic properties of SC-DDs. Nevertheless, very little knowledge exists for diamond concerning the well-known pulse-height defects in solid-state detectors. Therefore, in order to compare silicon- with diamond detectors we are using weakly-ionizing, mixed-nuclide alpha sources (<sup>239</sup>Pu, <sup>241</sup>Am, <sup>244</sup>Cm) of  $E_\alpha \sim$

5.5 MeV. The signals of D4 and of a silicon pin diode detector are processed with a charge-sensitive preamplifier[13], a spectroscopy shaping amplifier and a peak-sensing 13 bit ADC. The precision of the energy calibration is  $\delta E = \pm 1$  keV and the  $\alpha$ -resolution of the pin diode is 14 keV. The D4 spectrum shown in Figure 9 is obtained at positive bias and has been calibrated using a linear fit to the measured ratios of the amplitudes in both detectors  $R_{1,2,3} = A^{\text{Si}}(E_{1,2,3})/A^{\text{D}}(E_{1,2,3})$ . The fit gives a  $R^{\text{avg}} = 3.531 \pm 0.002$ .

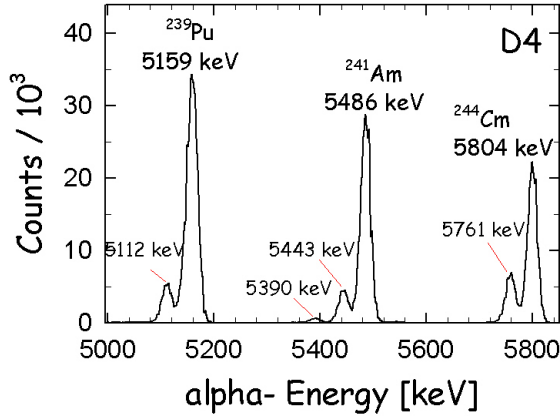


**Figure 9:**

Mixed nuclide  $\alpha$ -spectrum measured with D4. Energy resolution  $\Delta E = 17$  keV has been obtained and thus, all satellite  $\alpha$ -lines are distinguished. The silicon pin-diode detector used for calibration have shown  $\Delta E = 14$  keV in this test.

Since  $R^{\text{avg}}$  can be also written as  $R^{\text{avg}} = \epsilon^{\text{D4}}/\epsilon^{\text{Si}}$ , where  $\epsilon^{\text{D4}}$  and  $\epsilon^{\text{Si}}$  are the energies needed to create an e-h pair in the respective materials, a conversion factor  $\epsilon^{\text{D4}} = 12.78 \pm 0.03$  eV/e-h pair is extracted for this sample. Usually, a value of  $\epsilon^{\text{ref}} = 13.1$  eV/e-h is given[14]. The precision of the measured value is determined by the uncertainty of the chosen  $\epsilon^{\text{Si}}(300\text{K}) = 3.62 \pm 0.03$  eV/e-h pair[14].

An excellent energy resolution  $\Delta E = 17$  keV corresponding to a  $\Delta E/E = 0.003$  results for D4. Considering the higher Fano factor expected for DDs, this value is almost as good as the silicon detector resolution. For comparison, the highest-quality PC-DDs have a  $\Delta E/E=0.65$ [3].

#### 4.4 Charge-Collection Efficiency

The charge collected at positive and negative bias from the 5.486 MeV line of a pure  $^{241}\text{Am}$  source is plotted in Figure 10 versus the electric field. Pulser calibration of the charge-sensitive electronics has been applied in this case. Almost full saturation at much lower fields than in PC-DDs is obtained[3]. The charge collected from electrons reaches saturation at a higher field than is the case for holes. The dashed line indicates the charge expected for  $\epsilon^{\text{ref}} = 13.1$  eV/e-h. Obviously, this value is not valid for this data, which confirms perfectly the conversion factor of  $\epsilon^{\text{D}} = 12.78$  eV/e-h measured for D4 and the case of loss-less charge drift.

In order to test the CCE with relativistic particles in the laboratory, electrons from a  $^{90}\text{Sr}$  source ( $E_{\beta}^{\text{max}} = 2.217$  MeV) of an energy  $E_{\beta} > 1$  MeV have been used

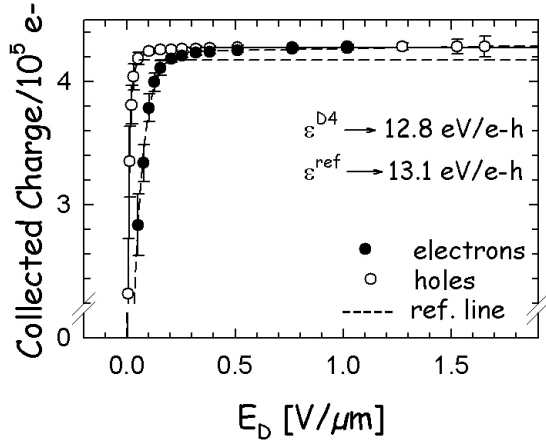


**Figure 10:**

Collected charge obtained from the 5.486 MeV  $\alpha$ -transition of a pure  $^{241}\text{Am}$  source, by operating D4 at positive bias (hole drift, open circles) and negative bias (electron drift, dots). In both cases the saturation charge confirms the measured  $\epsilon^{\text{D4}}$  value of 12.8 eV/e-h, whereas  $\epsilon^{\text{ref}} = 13.1$  eV/e-h (dashed line) underestimates the data.

in coincidence with a plastic-scintillator detector placed behind D4. The preliminary calibrated spectra obtained for positive- (solid line) and negative (dotted line) electric field  $E_D = \pm 0.5$  V/ $\mu\text{m}$  are shown in Figure 11. The mean value of the distribution corresponds to a collected charge of 16490 e, whereas the peak value, given by the scintillator threshold, corresponds to 14070 e. According Reference[15], 14150 e are expected on average from MIPs in a diamond detector of 393  $\mu\text{m}$  thickness. In any case, Figure 11 demonstrates the clear separation of the electron distribution from the electronic noise and confirms a CCE of almost 100% for traversing relativistic particles of  $Z = 1$ .

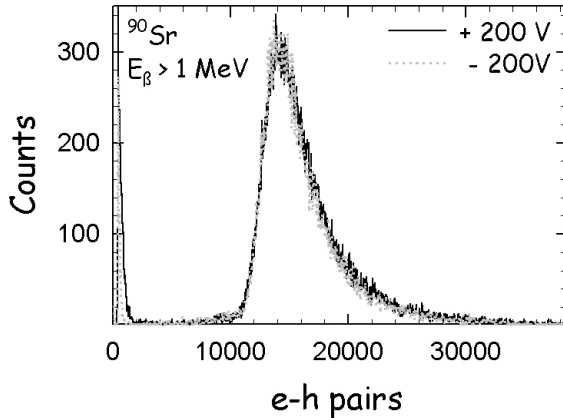


**Figure 11:** (Preliminary)

Collected charge spectrum of a  $^{90}\text{Sr}$  source measured with D4 at positive bias (solid black line) and negative bias (dotted grey line). Only electrons of energy higher than 1 MeV are accepted. The mean charge of 16490 e collected in both cases confirms a CCE  $\sim 100\%$  also for the case of relativistic particles of  $Z=1$ .

## 5 Summary and Conclusions

We tested four single-crystal CVD-diamond samples of various thicknesses and areas in the configuration of charged particle detectors. The dark-current characteristics at low bias reveal very low conductivity  $\ll 1$  nA/ $\text{mm}^3$ . However, the overall significance of these measurements is not yet completely understood. In particular, the role of the electrode contacts is still confusing. Some samples show increasing current (in the order of a few nA/ $\text{mm}^3$ ) at unexpectedly low

electric fields. This observation suggests surface conductivity and contact problems, which must be further investigated.

Extensive study has been made of the original diamond response to an impinging charged particle, as this contains all information about the electronic properties of a detector material. Broadband (1 MHz to 2.3 GHz) electronics has been used in order to maintain the ultra-fast diamond signals. We observed uniform pulses from fast, solid-state drift chambers of homogeneous electric field well suited for timing applications. The rise time is below 200 ps and the FWHM, depending on the detector thickness, in the order of a few nanoseconds. We expect therefore, similar timing properties as for PC-DD[3] but with slightly reduced rate capability and a significantly improved S/N ratio. The almost constant area of the timing pulses confirms impressively the excellent spectroscopic properties of early single-crystal CVD diamond detectors, found to be already comparable to silicon detectors. However, for low-background implementation of detectors in hadron-physics experiments the S/N ratio must be optimized at a minimum detector thickness. The high energy needed to create an e-h pair is therefore the only drawback found so far for single-crystal diamond detectors.

## Acknowledgment

This work is supported by the EU, Project RII3-CT-2004-506078. We express our gratitude to Element Six, Ascot UK for the generous provision of the SC-CVD diamond samples. We acknowledge the European Synchrotron Radiation Facility for provision of synchrotron radiation access on beamline ID21.

## References

---

- [1] W. Adam et al., The RD42 Collaboration, NIM A **511** (2003) 124
- [2] C. Mer et al., Diamond and Related Materials, **13** (2004) 791
- [3] E. Berdermann et al., Diamond and Related Materials **10** (2001) 1770
- [4] C. Nebel, Habilitationsschrift, TU München, 1998
- [5] Element Six, Ascot, Berkshire, UK
- [6] P. Bergonzo et al., Diamond and Related Materials **11** (2002) 418
- [7] P. Moritz et al., Diamond and Related Materials **10** (2001) 1765
- [8] C. Jacoboni et al., Solid State Electronics **20** (1977) 77
- [9] Pernegger et al., Journal of Applied Physics (2005)
- [10] Pomorski et al., phys.stat.sol (a) to be published
- [11] Lari et al., NIM A **537** (2005) 581
- [12] J. Isberg et al., Diamond and Related Materials **13** (2004) 872
- [13] Fo et al., CSTA2 TU Darmstadt
- [14] EG&G Ortec, "Modular Pulse-Processing Electronics and Semiconductor Radiation Detectors", #95, (1994)
- [15] D. Meier, PhD Thesis, University of Heidelberg (1999)